A Two-Stage Adaptive Control Rod Overlap Strategy for Load-Following Operation of a Soluble Boron-Free SMR

Chanwoo Kim[a], Deokjung Lee[a*]
[a]*Department of Nuclear Engineering, Ulsan National Institute of Science and Technology, 50 UNIST-gil, Eonyang-eup, Ulju-gun, Ulsan 44919, Republic of Korea*
[*]*Corresponding author: deokjung@unist.ac.kr*

***Keywords : Two-stage adaptive overlap strategy, load-following operations, soluble boron-free, SMR**

1. Introduction

The global transition toward carbon-neutral energy systems has significantly increased the penetration of renewable energy sources, resulting in larger fluctuations in power generation and growing demand for flexible power system operation. Consequently, nuclear power plants are increasingly expected not only to provide reliable baseload electricity but also to perform load-following operations (LFO) to compensate for the intermittency of renewable energy. In soluble boron-free (SBF) small modular reactors (SMRs), the boron-related functions of the chemical and volume control system are eliminated to simplify the reactor system and reduce liquid effluent. Consequently, core reactivity and power distribution must be controlled solely through burnable absorbers and control rods (CRs). During daily LFO, substantial insertion of CR banks is often required to compensate for the reactivity changes associated with large power reductions and subsequent power recovery. However, extensive CR insertion severely distorts the spatial power distribution by suppressing the neutron flux in the upper core region, shifting the axial power peak toward the bottom, and inducing local power peaking near the CR tips. Such spatial distortions worsen the axial shape index (ASI) and significantly reduce thermal-hydraulic safety margins, posing major challenges to fuel integrity and operational flexibility.

Conventionally, nuclear reactors employ a fixed-overlap strategy between adjacent control banks to simplify operations and calibration. Under this fixed framework, the overlapping distance between consecutive banks is held constant throughout the fuel cycle. Although easily implementable, the fixed overlap fails to accommodate the dynamic changes in core physics characteristics—such as burnable absorber depletion, fuel depletion distribution, and variations in axial CR worth—as burnup progresses from the beginning of cycle (BOC) to the end of cycle (EOC). Furthermore, during LFO, the reactivity control requirements under low-power conditions differ markedly from those at full-power. Applying an identical overlap length regardless of the operating state can lead to excessive or insufficient CR bank movement, resulting in degraded axial power control, severe ASI excursions, and elevated F_q.

To overcome these limitations, this study proposes a two-stage adaptive overlap strategy that dynamically adjusts the overlap length according to the operating condition by employing two optimized overlap configurations: a narrow overlap during LFO to restrict localized power distortion and a wider overlap during full-power operation (FPO) to stabilize the axial power profile.

The effectiveness of the adaptive overlap strategy is systematically evaluated for an SBF SMR using the STREAM/RAST-K two-step reactor physics code system [1, 2]. First, parametric evaluations under both low-power and full-power conditions are conducted to identify suitable overlap ranges for each operating mode. Based on these insights, representative narrow and wide overlap configurations are selected and integrated into a daily load-following maneuver across various burnup steps. The operational performance is comprehensively assessed in terms of ASI, F_q, and CR movement. The results demonstrate the potential of the proposed two-stage adaptive overlap strategy to mitigate axial power distortion during load-following maneuvers while maintaining effective reactivity control during power recovery.

2. Methodology

2.1. SMR Model

The SMR core consists of 69 fuel assemblies with an active core height of 240 cm. Each fuel assembly adopts a 17 × 17 Westinghouse-type configuration, containing UO_2 fuel pins with U-235 enrichment levels of up to 4.95%. Gd_2O_3 fuel pins with contents of up to 8.0 wt% are employed as burnable absorbers, with natural to 70% enriched Gd-155 and Gd-157 used to provide reactivity control throughout the fuel cycle [3]. Reactivity control is provided by 28-finger control element assemblies containing Ag-In-Cd (AIC) absorber material. Four regulating banks, designated R4, R3, R2, and R1 in the insertion sequence, are employed for power and reactivity control.

2.2. Regulating Bank Configuration and Overlap Definition

Four regulating banks are axially positioned within the 240 cm active core region to provide reactivity control and regulate the axial power distribution. The CR overlap length is defined as the axial distance over which

two adjacent regulating banks simultaneously occupy the active core region, as illustrated in Fig. 1. In the SMR model considered in this study, the reference CR overlap length is set to 50% of the active core height, corresponding to 120 cm.

The overlap consequently affects the axial distribution of CR worth. A narrow overlap causes multiple regulating banks to be positioned within a relatively narrow axial region, resulting in a more concentrated distribution of CR worth. In contrast, a wide overlap distributes the regulating banks over a broader axial range, leading to a more distributed axial control effect. Therefore, adjusting the overlap length provides an additional means of controlling the axial power distribution while maintaining the required reactivity control.

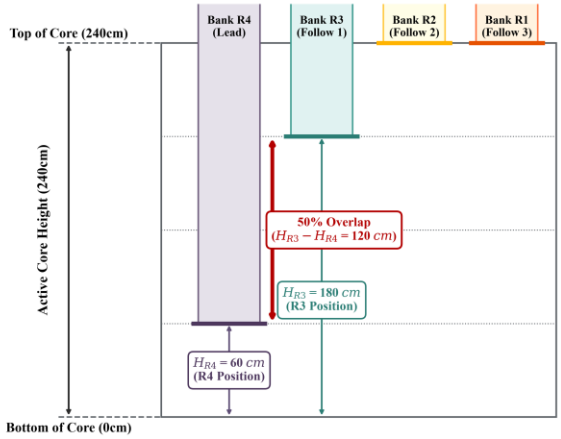


Fig. 1. Definition of CR overlap length.

2.3. Two-stage Adaptive Overlap Strategy

As discussed in the introduction, applying a conventional fixed-overlap strategy during LFO can lead to inefficient reactivity control due to dynamic changes in the core. To effectively address this, the proposed two-stage adaptive overlap strategy dynamically adjusts CR overlap length based on the specific operating phase.

The proposed strategy employs two target overlap configurations: a narrow overlap (L_{narrow}) for power-reduction, low-power, and early power-recovery phases, and a wide overlap (L_{wide}) for FPO. During the power-reduction and low-power phases, the narrow overlap configuration is employed to provide effective axial power control under deep CR insertion. During the early stage of power recovery, L_{narrow} is initially retained to avoid abrupt changes in the axial power distribution while the core undergoes transient power and xenon redistribution. As the reactor approaches FPO, the overlap length is gradually increased toward L_{wide}, which is subsequently maintained to provide an appropriate axial power distribution during FPO.

A direct transition between L_{narrow} and L_{wide} at the boundary between operating conditions can cause abrupt changes in the axial power distribution and undesirable ASI excursions. To mitigate such discontinuities, a gradual overlap transition mechanism is introduced. Under this mechanism, the overlap length is increased stepwise from L_{narrow} through a series of intermediate overlap configurations, denoted as L_1, L_2, and L_3, until the target wide overlap L_{wide} is reached. The overlap transition is therefore expressed as $L_{narrow} \rightarrow L_1 \rightarrow L_2 \rightarrow L_3 \rightarrow L_{wide}$.

The transition is initiated during the later stage of power recovery and continues through the initial stabilization phase of FPO. Extending the overlap transition beyond the point at which the reactor reaches 100% power allows the axial power distribution to evolve gradually during the transition from LFO to FPO. For the transition period ($t_{start} \leq t \leq t_{end}$), the overlap length is defined as

$$L(t) = L_{narrow} + \left[\frac{L_{wide} - L_{narrow}}{t_{end} - t_{start}}\right](t - t_{start}) \quad (1)$$

Figure 2 schematically illustrates the relationship between the reactor power and the corresponding CR overlap throughout the 24 h daily LFO maneuver. As depicted, the overlap length is gradually increased from L_{narrow} to L_{wide}, passing through the intermediate configurations from the later stage of power recovery through the initial phase of FPO. In the present calculations, the overlap transition described by Eq. (1) is applied through discrete stepwise adjustments at 0.5 h intervals between 11.0 h and 13.0 h. The intermediate configurations (L_1–L_3) are evaluated directly using Eq. (1) at their respective time steps, with the resulting continuous values rounded down to the nearest integer to accommodate the 1 cm control resolution.

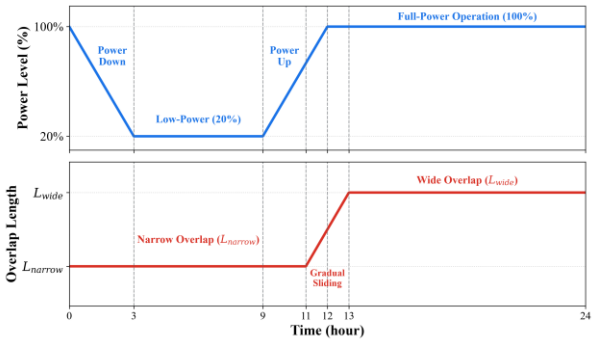


Fig. 2. Reactor power profile and corresponding adaptive overlap length trajectory during the 24 h daily LFO.

2.4. Core Simulation and Daily Load-Following Scenario

The core simulations are performed using the two-step code system STREAM/RAST-K [1, 2], with nuclear cross-section data generated from the ENDF/B-VII.1 library. The core behavior during the daily LFO is evaluated using a quasi-static method with a uniform

time step (Δt) of 30 minutes (0.5 h). To accurately capture the initial conditions prior to the power variation, the equilibrium xenon concentration is explicitly solved for the first quasi-static step. Furthermore, thermal-hydraulic feedback is consistently incorporated into all time-dependent calculations to account for the coupled neutronic and thermal-hydraulic effects during power variations. During each quasi-static step, the critical positions of the regulating banks are determined through a criticality search.

The operational simulation assumes a 24 h daily load-following scenario characterized by a 100-20-100% power profile. The specific sequence of the power schedule is defined as follows: a linear power reduction from 100% to 20% over 3 h (0–3 h), low-power operation at 20% for 6 h (3–9 h), a linear power recovery to 100% over 3 h (9–12 h), and FPO at 100% for the remaining 12 h (12–24 h).

To comprehensively verify the effectiveness of the proposed control strategy throughout the core lifetime, the 24 h LFO is simulated at six representative burnup steps. Expressed in MWd/kg, these selected evaluation points are the beginning of cycle (BOC, 0), early fuel cycle (EFC, 5), middle of cycle (MOC, 10), late middle of cycle (LMOC, 15), late fuel cycle (LFC, 17), and end of cycle (EOC, 21.38). Although LFO is not typically performed near EOC due to the restricted reactivity control margin and heavily depleted core conditions, the EOC evaluation is intentionally included to provide a conservative assessment of the proposed strategy under the most challenging core state.

3. Results

To evaluate the core performance under the proposed two-stage adaptive overlap strategy, comprehensive simulations were conducted across all six representative burnup states throughout the fuel cycle. For clarity and concise presentation, the detailed 24 h operational behaviors are primarily discussed focusing on three characteristic stages: BOC, MOC, and EOC.

3.1. Parametric Analysis of CR Overlap

To establish the basis for the proposed adaptive overlap strategy, systematic parametric sweeps of the CR overlap length were performed to identify the target overlap configurations for different operating conditions. With an active core height of 240 cm, the overlap length was varied from 30 to 210 cm, corresponding to 12.5%–87.5% of the active core height. This range was selected as the practical search range to cover the relevant overlap configurations while maintaining distinct bank-wise reactivity control.

Figure 3 presents 2D contour maps of F_q and |ASI| as functions of LFO time and CR overlap length at BOC, MOC, and EOC. The results show that the favorable overlap region shifts with the operating power. During the reduced-power phase (3–9 h), a relatively narrow overlap is preferred to limit axial power redistribution under deep CR insertion. In contrast, a wider overlap is favorable during the full-power recovery and stabilization phase (12–24 h), where it distributes the CR worth over a broader axial region and mitigates localized power peaking near the CR tips. Consequently, a single fixed overlap, such as the conventional 120 cm configuration, cannot provide the same level of axial power control throughout the entire LFO maneuver.

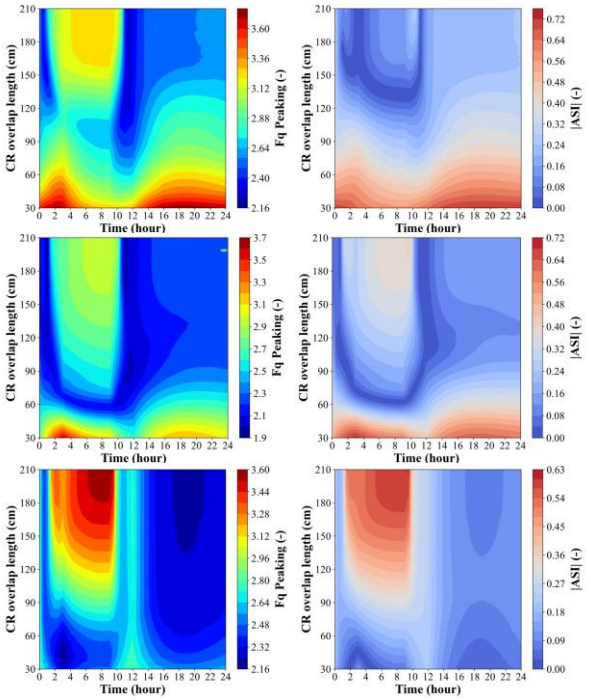


Fig. 3. Parametric sweep contour maps of F_q and |ASI| at BOC, MOC, and EOC (from top to bottom).

To quantitatively determine the target overlap lengths, a constrained minimax optimization formulation was applied separately to the reduced-power and full-power phases. The search space is first filtered using ASI criteria to ensure axial stability, and the optimal overlap length minimizing F_q is subsequently selected:

$$L^*_{\text{narrow}} = \arg\min_{L\in\mathcal{S}_{\text{narrow}}} \left\{ \max_{t\in\mathcal{T}_{\text{LFO}}} F_q(L,t) \right\} \tag{2}$$

$$\text{where } \mathcal{S}_{\text{narrow}} = \left\{ L \;\middle|\; \max_{t\in\mathcal{T}_{\text{LFO}}} |\,\text{ASI}(L,t)| \le 0.1 \right\}$$

$$L^*_{\text{wide}} = \arg\min_{L\in\mathcal{S}_{\text{wide}}} \left\{ \max_{t\in\mathcal{T}_{\text{FPO}}} F_q(L,t) \right\} \tag{3}$$

$$\text{where } \mathcal{S}_{\text{wide}} = \left\{ L \;\middle|\; \max_{t\in\mathcal{T}_{\text{FPO}}} |\,\text{ASI}(L,t) - \text{ASI}_{\text{eq}}| \le 0.05 \right\}$$

where ASI_{eq} denotes the burnup-dependent equilibrium ASI under the 100% full-power condition. Here, the equilibrium state refers to the short-term xenon equilibrium at full power rather than a long-term cycle

equilibrium. The evaluation time windows are defined as $\mathcal{T}_{\mathrm{LFO}} = [0,11]$ h for the power reduction, low-power, and early recovery phase, and $\mathcal{T}_{\mathrm{FPO}} = [13,24]$ h for the full-power stabilization phase. The ASI target bands of ± 0.10 during LFO and ± 0.05 during FPO are selected, where the LFO target is set to a wider margin to accommodate the larger transient ASI fluctuations expected during power-level variations. In cases where no overlap length strictly satisfies the standard target band (e.g., at BOC where the core exhibits a strong positive ASI bias throughout LFO), the constraint is relaxed to minimize the deviation from $\mathrm{ASI}_{\mathrm{eq}}$, and the overlap minimizes F_q is selected.

Based on this optimization framework, the optimal narrow-overlap targets for the reduced-power phase are determined to be 112, 64, and 59 cm at BOC, MOC, and EOC, respectively, while the corresponding wide-overlap targets for the full-power phase are 153, 132, and 120 cm. These results demonstrate that the preferred overlap configuration depends on both the operating power and burnup state. Accordingly, the resulting target pairs, L^{*}_{narrow} and L^{*}_{wide}, were adopted as the basis for the proposed two-stage adaptive overlap strategy.

3.2. Load-Following Performance Evaluation

Using the target overlap configurations identified from the parametric sweep analysis, daily load-following simulations were performed across the cycle. For concise visualization, Figure 4 compares the transient behaviors of ASI, F_q, regulating bank positions, and the axial shape index of the Xe-135 number density ($\mathrm{ASI}_{\mathrm{Xe}}$) for the fixed and adaptive overlap strategies at BOC, MOC, and EOC. The corresponding performance metrics for all six representative burnup states are summarized in Table I. In Figure 4, the shaded regions demarcate the distinct phases of the daily load-following cycle: the gray-shaded regions from 0 to 3 h and from 9 to 12 h represent the power de-escalation (ramp-down) and escalation (ramp-up) transient phases, respectively, while the light-blue-shaded region from 3 to 9 h denotes the low-power steady-state operation phase. The unshaded region from 12 to 24 h corresponds to the FPO phase.

The adaptive strategy generally reduces the axial power redistribution during the reduced-power and power-recovery phases by employing a narrower overlap than the fixed 120 cm configuration. As summarized in Table I, the peak-to-peak ASI variation is reduced by 26.1%, 16.2%, 12.2%, 13.4%, 32.2%, and 54.1% at BOC, EFC, MOC, LMOC, LFC, and EOC, respectively.

The $\mathrm{ASI}_{\mathrm{Xe}}$ behavior further demonstrates the effect of the preceding load-following history. At EOC, the adaptive strategy produces a slightly more negative $\mathrm{ASI}_{\mathrm{Xe}}$ during the low-power period, reaching approximately -0.148 at 9 h compared with -0.133 for the fixed-overlap strategy. During power recovery, however, the adaptive case recovers more rapidly, and its $\mathrm{ASI}_{\mathrm{Xe}}$ becomes less negative after approximately 13 h. Thus, the adaptive strategy does not simply minimize the instantaneous xenon asymmetry but modifies the axial Xe-135 distribution and its subsequent evolution through the load-following history.

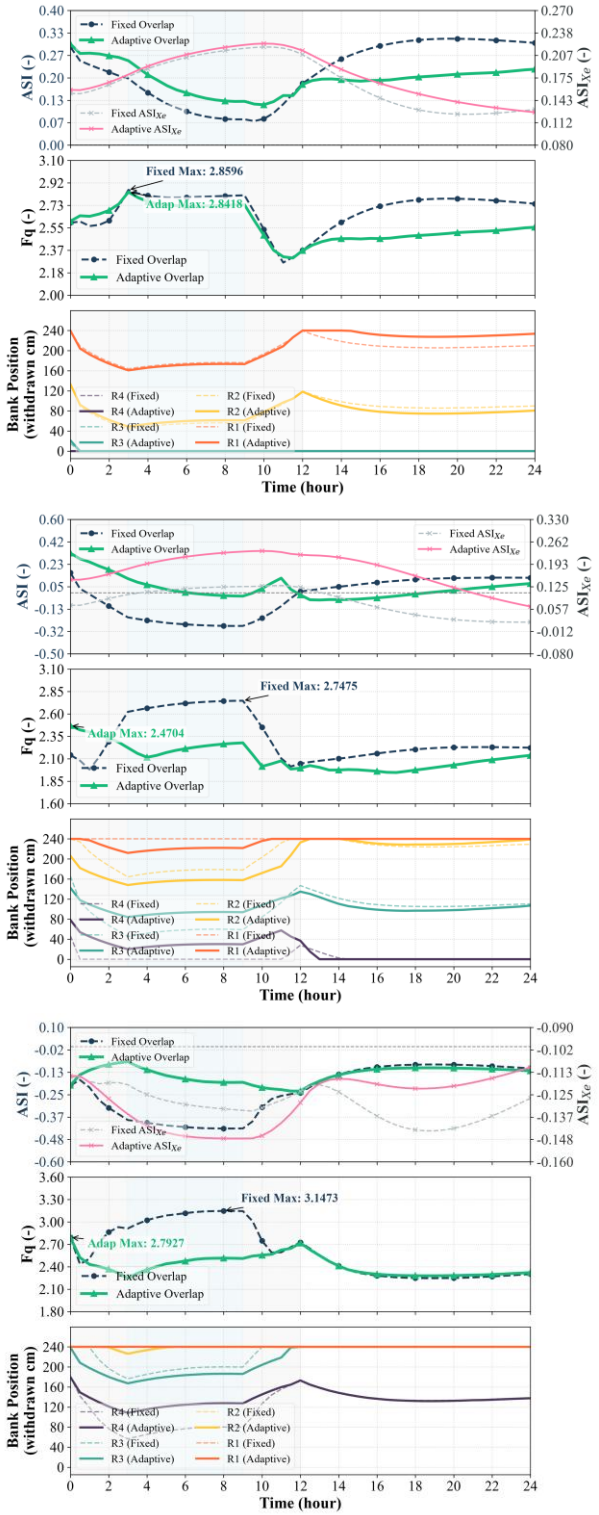


Fig. 4. 24 h daily LFO trajectories of ASI, F_q, regulating bank positions, and $\mathrm{ASI}_{\mathrm{Xe}}$ under fixed and adaptive overlap strategies at BOC, MOC, and EOC (from top to bottom).

This history effect is particularly evident during the EOC full-power period. Although both strategies eventually use the same $L^*_{\text{wide}} = 120$ cm overlap, their ASI and F_q responses do not immediately become identical. The different overlap configurations applied during the preceding power reduction and recovery phases result in different axial power and Xe-135 distributions when the reactor enters the full-power condition. Therefore, the reactor retains a different state even after the overlap length becomes identical. As a result, the EOC maximum F_q decreases from 3.1473 for the fixed-overlap strategy to 2.7927 for the adaptive strategy, corresponding to an 11.27% reduction.

At LMOC, the adaptive strategy produces a slight increase of 1.39% in the maximum F_q, from 2.6831 to 2.7204. This behavior is attributed to the more concentrated CR worth associated with the narrower 88 cm overlap, which can induce localized flux peaking during deep bank insertion. In evaluating F_q, the absolute thermal loading should be considered together with the relative power peaking. Because the reactor considered in this study has a lower average linear power density than typical commercial reactors, a given absolute thermal limit permits a larger relative power peaking. Furthermore, during reduced-power operation, the lower overall reactor power provides additional thermal margin compared with FPO. Therefore, the allowable relative power peaking during load-following operation can be higher than corresponding to the full-power condition. Based on these considerations, an F_q target criterion of 3.2 was conservatively adopted for the present load-following evaluation. All evaluated cases satisfy this criterion, with the maximum F_q of 3.1473 occurring at EOC for the fixed-overlap strategy and decreasing to 2.7927 with the adaptive strategy.

Table I: Comparison of Core Performance Metrics Between Fixed and Adaptive Overlap Strategies

Burnup (MWd/kg)	Strategy	Overlap ($L_{narrow} \rightarrow L_{wide}$, cm)	Max. Fq	Max. Fq Relative Change (%)	ASI Range	ASI Range Relative Change (%)
BOC (0.0)	Fixed	120	2.8596	-	0.071 to 0.316	-
	Adaptive	**112 → 153**	**2.8418**	**-0.62**	**0.120 to 0.301**	**-26.1**
EFC (5.0)	Fixed	120	2.8261	-	-0.193 to 0.158	-
	Adaptive	**79 → 130**	**2.5363**	**-10.25**	**-0.028 to 0.266**	**-16.2**
MOC (10.0)	Fixed	120	2.7475	-	-0.272 to 0.164	-
	Adaptive	**64 → 132**	**2.4704**	**-10.09**	**-0.059 to 0.324**	**-12.2**
LMOC (15.0)	Fixed	120	2.6831	-	-0.258 to 0.265	-
	Adaptive	**88 → 131**	**2.7204**	**+1.39**	**-0.121 to 0.332**	**-13.4**
LFC (17.0)	Fixed	120	2.9003	-	-0.352 to 0.186	-
	Adaptive	**67 → 108**	**2.6501**	**-8.63**	**-0.057 to 0.308**	**-32.2**
EOC (21.38)	Fixed	120	3.1473	-	-0.426 to -0.093	-
	Adaptive	**59 → 120**	**2.7927**	**-11.27**	**-0.232 to -0.079**	**-54.1**

3.3. CR Maneuverability and Cumulative Bank Travel

Figure 5 presents the cumulative displacement of the regulating CR banks during the 24 h LFO cycle, where one step corresponds to 1 cm of axial displacement. Under the conventional fixed-overlap strategy, repeated compensatory CR movements are observed throughout the maneuver. The fixed overlap cannot fully accommodate the changing axial reactivity requirements during power variation, resulting in frequent rod repositioning to maintain criticality and axial power constraints.

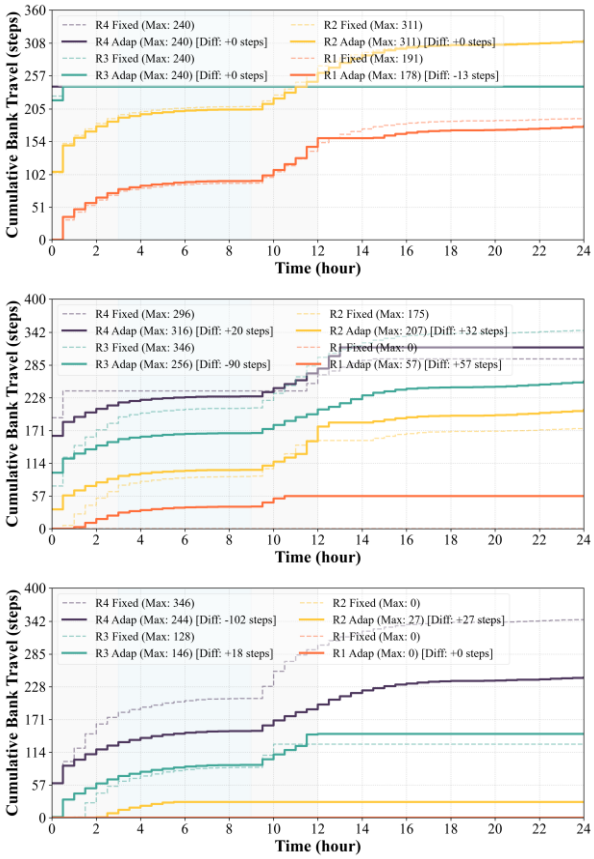


Fig. 5. Comparison of cumulative bank travel during the 24 h LFO at BOC, MOC, and EOC (from top to bottom).

Table II: Comparison of Cumulative Bank Travel Between Fixed and Adaptive Overlap Strategies

Burnup (MWd/kg)	Strategy	Overlap ($L_{narrow} \rightarrow L_{wide}$, cm)	Cumulative Bank Travel (steps)	Cumulative Bank Travel Relative Change (%)
BOC (0.0)	Fixed	120	982	-
	Adaptive	**112 → 153**	**969**	**-1.32**
EFC (5.0)	Fixed	120	901	-
	Adaptive	**79 → 130**	**851**	**-5.55**
MOC (10.0)	Fixed	120	817	-
	Adaptive	**64 → 132**	**836**	**+2.33**
LMOC (15.0)	Fixed	120	781	-
	Adaptive	**88 → 131**	**779**	**-0.26**
LFC (17.0)	Fixed	120	737	-
	Adaptive	**67 → 108**	**710**	**-3.66**
EOC (21.38)	Fixed	120	474	-
	Adaptive	**59 → 120**	**417**	**-12.03**

In contrast, the proposed stepwise overlap transition reduces unnecessary CR adjustments by gradually shifting the regulating configuration between L^*_{narrow} and L^*_{wide}. As summarized in Table II, cumulative bank travel is reduced at BOC, EFC, LMOC, LFC, and EOC by 1.32%, 5.55%, 0.26%, 3.66%, and 12.03%, respectively, with the largest reduction observed at EOC (from 474 to 417 steps). Although a slight increase of 2.41% is observed at MOC (from 817 to 836 steps), the adaptive strategy generally reduces cumulative CR movement

across the fuel cycle. These results indicate that adaptive overlap control alleviates excessive CR actuation during daily load-following, thereby reducing CR maneuvering demands and improving the overall control performance of the regulating system.

4. Conclusions

This study proposed a two-stage adaptive CR overlap strategy to improve axial power control and CR maneuverability during daily LFO of a soluble boron-free SMR. Unlike the conventional fixed overlap approach, the proposed strategy employs burnup specific narrow and wide overlap configurations during the reduced and full-power phases, respectively, with a gradual transition between the two target states.

The parametric analysis showed that the optimal CR overlap depends on both the operating condition and the burnup state. A narrow overlap (L^*_{narrow}) is favorable during deep CR insertion at reduced power to mitigate excessive axial power redistribution, whereas a wider overlap (L^*_{wide}) is more effective for distributing CR worth and limiting local pin peaking during FPO. These results indicate that a single fixed overlap configuration cannot effectively accommodate the changing axial control requirements throughout the load-following maneuver.

Compared with the conventional fixed 120 cm overlap strategy, the proposed adaptive strategy reduced the peak-to-peak ASI range by 12.2%–54.1% across the evaluated fuel cycle, with the largest reduction achieved at EOC. Furthermore, all maximum F_q were maintained safely below the adopted target criterion of 3.2. At EOC, the favorable axial Xe-135 evolution governed by the preceding low-power history contributed to an 11.27% reduction in the maximum F_q (from 3.1473 to 2.7927), significantly enhancing core thermal margins. In addition, the gradual overlap transition eliminated unnecessary compensatory rod movements, reducing cumulative regulating bank travel at most burnup states, with a maximum reduction of 12.03% at EOC.

Overall, the proposed adaptive overlap strategy improves core operational stability, preserves thermal safety margins, and enhances CR maneuverability by adapting the overlap configuration to dynamic axial control requirements. The results demonstrate its strong potential to provide a practical and robust control framework for flexible operations in soluble boron-free SMRs. While this study confirmed the effectiveness of the proposed framework based on a representative load-following maneuver, evaluating the strategy across more diverse and complex transient scenarios remains an essential next step. Accordingly, subsequent research will investigate a wide range of operational conditions and load-demand histories to systematically verify the strategy's robustness, enhance control adaptability, and ensure comprehensive core safety over the entire operational lifetime.

ACKNOWLEDGEMENT

This work was supported by Local Government (Ulsan) (2025).

REFERENCES

[1] S. Choi, D. Lee, Three-dimensional method of characteristics/diamond-difference transport analysis method in STREAM for whole-core neutron transport calculation, Computer Physics Communications, Vol. 260, 107332, 2021.
[2] J. Park, et al., RAST-K v2—Three-Dimensional Nodal Diffusion Code for Pressurized Water Reactor Core Analysis, Energies, Vol. 13, 6324, 2020.
[3] C. Kim, et al., Core Design Study for Soluble Boron-Free and Long-cycle Operation of Small Modular Reactor using Enriched Gadolinia, KNS Autumn Meeting, Changwon, Korea, October 24-25, 2024.